Prediction of macroscopic findings of hepatocellular carcinoma on hepatobiliary phase of gadolinium-ethoxybenzyl-diethylenetriamine pentaacetic acid-enhanced magnetic resonance imaging: Correlation with pathology

Yasunari Fujinaga[1)], Masumi Kadoya[1)], Kazuto Kozaka[2)], Rieko Shinmura[2)], Osamu Matsui[2)], Tadatoshi Takayama[3)], Masakazu Yamamoto[4)], Norihiro Kokudo[5)], Seiji Kawasaki[6)], Shigeki Arii[7)]

1) Department of Radiology, Shinshu University School of Medicine

2) Department of Radiology, Kanazawa University School of Medicine

3) Department of Digestive Surgery, Nihon University School of Medicine

4) Department of Surgery, Institute of Gastroenterology, Tokyo Women's Medical University

5) Department of Hepatobiliary and Pancreatic Surgery, University of Tokyo

6) Department of Hepato-biliary Pancreatic Surgery, Juntendo University School of Medicine

7) Department of Hepato-Biliary-Pancreatic Surgery, Tokyo Medical and Dental University

Corresponding author:

Yasunari Fujinaga

Department of Radiology, Shinshu University School of Medicine

3-1-1 Asahi, Matsumoto, Japan 390-8621

Tel: +81-263-37-2650; Fax: +81-263-37-3081

e-mail: fujinaga@shinshu-u.ac.jp

Abstract

Aim: We aimed to correlate the macroscopic and magnetic resonance imaging (MRI) findings of hepatocellular carcinomas (HCC). Methods: This was a multicenter study, whose study protocol was approved by each Institutional Review Board. One hundred and forty-six resected nodules in 124 patients who were received preoperative hepatobiliary phase of gadolinium-ethoxybenzyl-diethylenetriamine pentaacetic acid-enhanced MRI (EOB-MRI) were analyzed. In both findings, we compared the diameter of HCC and macroscopic types divided into 5 types: (i) small nodular type with indistinct margin (SN-IM); (ii) simple nodular type (with distinct margin) (SN-DM); (iii) simple nodular type with extranodular growth (SN-EG); (iv) confluent multinodular type (CMN); and (v) infiltrative type (IF). Results: The diameters in each finding (D_{surg} and D_{MRI}) were significantly correlated (R=0.961), although D_{surg} was larger than D_{MRI} (P=0.0216). There were significant differences between D_{surg} in SN-IM and the other groups (P<0.0001). Sensitivity, specificity and accuracy were 5.3, 99.2 and 87; 84.8, 62.7 and 81.4; 58.1, 91.3 and 84.2; 70.6, 91.5 and 89, in SN-IM, SN-DM, SN-EG and CMN, respectively. The kappa value of every size was as follows: all sizes,

0.45; 20 mm or less, 0.23; more than 20 mm, 0.56. Conclusions: EOB-MRI could predict the macroscopic pathological findings except for SN-IM. Small tumor size might be helpful to diagnose SN-IM.

Key words

gadolinium-ethoxybenzyl-diethylenetriamine pentaacetic acid, hepatocellular carcinoma, macroscopic findings, magnetic resonance imaging, pathology

Introduction

Hepatocellular carcinoma (HCC) is one of the most common neoplasms in Japan, and its incidence has been increasing in the United States and Europe as well. [1] Pathologically, HCCs exhibit morphologic polymorphism and are classified into five types based on their macroscopic findings. [2] Because these types show an intense correlation with the prognosis of HCC including tumor recurrence and/or survival rate, [3-7] it is important to determine the macroscopic type of HCCs by imaging.

Post-vascular phase of sonazoid-enhanced ultrasonography has been reported as one of the useful methods to predict macroscopic findings.[8] On the other hand, magnetic resonance imaging (MRI) is one of the methods to assess liver tumors objectively. Gadolinium ethoxybenzyldiethylenetriamine pentaacetic acid (Gd-EOB-DTPA) is one of the hepatocyte-specific agents available for MRI. It is selectively taken up by functioning hepatocytes and shortens T1-relaxasation times of the liver. [9] It provides high detectability of liver tumors, such as HCC and metastatic liver tumors because it is usually not taken up by tumor cells. [10-12] In this manner, contrast-enhanced MRI using Gd-EOB-DTPA (EOB-MRI) can clearly demonstrate the border between the tumor and

the surrounding liver parenchyma, and has the potential to accurately predict the macroscopic types of HCCs.

In the present study, we correlated the macroscopic MR findings of HCCs to clarify this issue.

Methods

The study protocol of this multicenter study was approved by each institutional review board. Written informed consent was obtained from all participating patients before the MRI examinations and surgical operation.

Patients

Between 2008 and 2009, a total of 233 patients, whose liver nodules were wholly resected and histologically diagnosed with HCC, from 11 Japanese institutions were enrolled in this study. Patients selection was based on the following inclusion criteria: (i) macroscopic findings of histopathological reports could be reviewed (15 patients were excluded); (ii) EOB-MRI was performed with fat-suppressed T1-weighted

sequences, and MR images of hepatobiliary phase were acquired (77 patients were excluded); (iii) no treatment such as transcatheter arterial embolization or radiofrequency ablation was performed (16 patients were excluded). In addition, tumors including other cell types, such as cholangiocellular carcinoma and cholangiolocellular carcinoma were excluded (one patient was excluded). Finally, 146 nodules (range of diameter, 1–125 mm) of 124 patients (100 men and 24 women; age range, 38–84 years; average age, 66.9 years) were selected for the purpose of this study.

There were 22 patients infected with hepatitis B virus, 70 with hepatitis C virus, one with both hepatitis B and C virus, four with alcoholic liver disease and four with non-alcoholic steatohepatitis (NASH). The etiology of the HCCs in the other 23 patients was uncertain. Liver function was evaluated with the Child-Pugh classification system, with 117 patients classified as A, 7 patients as B.

MRI

All of the participating institutions had high-field-strength (1.5- or 3-T) MRI systems (Magnetom Vision [Siemens Medical Systems, Erlangen, Germany],

Magnetom Trio [Siemens], Achieva [Philips Medical Systems, Best, the Netherlands], Intera [Philips] and Signa HDx [GE Medical Systems, Milwaukee, WI] and used a phased array surface coil covering the whole liver.

Contrast-enhanced MRI was performed using Gd-EOB-DTPA at a dose of 0.1 mL/kg bodyweight. MRI of the hepatobiliary phase was obtained more than 15 minutes after contrast agent injection. Hepatobiliary phase contrast-enhanced MRI was obtained using 2-D (36 patients) or 3-D (88 patients) gradient echo (GRE) sequences with fat suppression. The parameters of the sequences in each institution were various because of differences in the MR systems used. Slice thickness was 6–8 mm in 2-D-GRE sequences and 3–4.8 mm in 3-D-GRE sequences.

Definition of macroscopic findings

We divided the macroscopic findings into five types based on the general rules of the clinical and pathological study of primary liver cancer in Japan [2] as follows: (i) small nodular type with indistinct margin (SN-IM); (ii) simple nodular type (with distinct margin) (SN-DM); (iii) simple nodular type with extranodular growth (SN-EG); (iv)

confluent multinodular type (CMN); and (v) infiltrative type (IF) (Fig. 1). In general, SM-IM type tumors do not differ greatly from background cirrhosis, and most are observed as indistinct nodules of 1.0–1.6 cm in diameter. SN-DM are observed as round tumors with distinct margin. SN-EG type tumors are observed as round tumors with extranodular growth, so called “budding”. CMN type tumors are observed as lobulated tumors consisting of multiple nodular lesions. IF type tumors appears as yellowish white lesions distinct from the surrounding liver tissues, but their infiltrative growth results in an irregular margin. We reviewed the pathological findings that were reported by the pathologists in each institution, and analyzed the tumor type and size. We considered the maximum diameter of the tumor as the tumor size (D_{surg}) in surgical specimens.

Pathological assessment was performed by one or two pathologists in each institution.

MR imaging analysis

On the hepatobiliary phase of EOB-MRI, maximum diameters of the tumors were

measured by four radiologists randomly, and were considered as the tumor size (D_{MRI}).

The MR findings of the tumors at the hepatobiliary phase were classified into five types along with the macroscopic types. Diagnostic criteria of each type are as follows: (i) SN-IM type tumors are round with an obscure margin (Fig. 1a); (ii) SN-DM type tumors are round with a clear margin (Fig. 1b); (iii) SN-EG type tumors are round with a clear margin and a focally protruding area (Fig. 1c); (iv) CMN type tumors are lobulated tumors with a clear margin (Fig. 1d); and (v) IF type tumors are lobulated tumors with an unclear margin. MRI was assessed by four radiologists (with 12, 15, 18 and 33 years' experience of abdominal diagnosis, respectively) independently. When the assessed type was not unanimously agreed upon, the reviewers assessed together and to discussed to reach consensus. All MRI was reviewed with a commercial software package, EV insite (PSP, Tokyo, Japan). The MRI was read blind, with none of the readers having any information regarding the patients' clinical background or their pathological findings. Four radiologists assessed the MR images at the slice of the maximum tumor dimension and categorized the tumors into five types as with the pathological types.

In this study, we did not assess pre-contrast and early phase of dynamic contrast-enhanced MR images because of obscurity and inhomogeneity of the nodules.

Statistical analysis

Statistical analyses were performed with a statistical software package (Prism, version 5 [GraphPad Software, California, USA] and Microsoft Excel 2008 [Microsoft, Redmond, WA, USA]). The Spearman's rank correlation coefficient and paired Student's *t*-test were used to examine the association between D_{surg} and D_{MRI}. The MRI determinations of each group were compared with the pathological macroscopic findings, and the diameters were compared using the Kruskal-Wallis test and Dunn's multiple comparison test, and sensitivity, specificity, accuracy, positive predict value (PPV) and negative predict value (NPV) of each type, as well as concordance rate using kappa statistics, were calculated. A kappa value of 0.20 or less indicated poor agreement; 0.21–0.40, fair agreement; 0.41–0.60, moderate agreement; 0.61–0.80, good agreement; and 0.81–1.00, excellent agreement. Values of $P < 0.05$ were regarded as statistically significant.

Results

The mean value and 95% confidence interval (CI) for the correlation coefficient between D_{surg} and D_{MRI} were 0.961 (95% CI = 0.946–0.972) (Fig. 2). The median diameter (range) of D_{surg} and D_{MRI} were 25 (1–125) and 24.5 (2–130) mm, respectively. The differences between both means of diameter were significant ($P = 0.0216$).

Table 1 shows the correlation between the macroscopic and MR findings of HCCs. Pathologically and radiographically, there were 19 nodules and two nodules in SN-IM, 79 and 92 in SN-DM, 31 and 28 in SN-EG and 17 and 23 in CMN, and 0 and 1 in IF, respectively. The concordance rate was highest in SN-DM and lowest in SN-IM. On MRI, 15 of 19 SN-IM nodules were misdiagnosed as SN-DM, seven of 79 SN-DM nodules as SN-EG, seven of 31 SN-EG nodules as SN-DM and three of 17 CMN nodules as SN-DM.

Table 2 shows the sensitivity, specificity, accuracy, NPV and PPV of each group. In comparisons among the groups, sensitivity was highest in SN-DM, specificity in SN-IM, accuracy in CMN, NPV in CMN, and PPV in SN-DM.

On EOB-MRI, the diameter of the tumor was 20 mm or less in 51 nodules (small group). Sixteen of these nodules were pathologically diagnosed as SN-IM, 27 as SN-DM, seven as SN-EG and one as CMN. The diameter of the tumor was more than 20 mm in 95 nodules (large group). Of these, three nodules were pathologically diagnosed as SN-IM, 52 as SN-DM, 24 as SN-EG and 16 as CMN. When we classified them into 2 subgroups with a dividing lime of 20 mm in diameter, the calculated statistics were changed (Table 2). In SN-IM group, sensitivity was low in each subgroup, while accuracy was high in the large group because of the large number of true negatives (n = 92). In SN-DM group, specificity and accuracy of the large group were higher than those of the small group. In SN-EG and CMN groups, specificity and accuracy were comparable. When the SN-IM in each group (MRI and pathological findings) was excluded, sensitivity, specificity and accuracy of SN-IM were 73.6, 79.1 and 75.5, respectively. In this selection, we classified the tumors into two subgroups, 2-D-GRE and 3-D-GRE group, and statistics in each group were as follows: sensitivity, 81.8 and 89.1; specificity, 71.4 and 77.8; and accuracy, 77.8 and 84.6.

The kappa values of every size were as follows: all sizes, 0.45; 20 mm or less, 0.23;

more than 20 mm, 0.56. When the SN-IM in each group (MRI and pathological findings) was excluded, the kappa value was improved (all size, 0.58; 20 mm or less, 0.53; more than 20mm, 0.58), and that in 2-D-GRE and 3-D-GRE group was 0.48 and 0.61, respectively.

The median (range) of D_{MRI} in SN-IM, SN-DM, SN-EG and CMN were 12 (4–23) mm, 25 (9–105), 28 (13–125) and 29 (18–95), respectively. There was a significant difference between D_{MRI} in SN-IM and the other groups (P<0.0001), but no significant differences in D_{MRI} between SN-DM, SN-EG and or CMN (Fig. 3).

Discussion

Independent prognostic factors for recurrence and survival after HCC resection include tumor size, vascular invasion, intrahepatic metastasis, fibrosis and cirrhosis. [7, 13-18] Macroscopic type is also one predictor of survival rate or recurrence rate. [3-7] EOB-MRI is one useful tool to assess these factors because it provides higher sensitivity and higher detectability than computed tomography. [10-13] However, it has been unclear whether the shape of the tumor is shown accurately on hepatobiliary phase

MRI.

As for tumor size, a strong correlation between D_{surg} and D_{MRI} was noted in this study. So the diameter of the tumor can be assumed by EOB-MRI. However, it should be recognized that the diameter of the tumor on EOB-MRI may be underestimated because D_{MRI} tended to be slightly smaller than D_{surg}. We attributed this to a partial volume effect due the use of thick slices relative to the small tumor size.

This is the first report to correlate the macroscopic and MR findings of HCC. Our results demonstrated that most HCC with an indistinct margin demonstrated a distinct margin on MRI, while the sensitivity of SN-IM was very low in all tumor sizes. We attributed this result to the excellent contrast between tumor and the adjacent normal liver, as well as a limitation of the image resolution for small tumors. This problem is minor because both SN-IM and SN-DM can be expected to have a good prognosis. It is important to detect extranodular growth because of the increased frequency of vascular invasion and tumor spread. [3] Vascular invasion and intrahepatic metastasis are more frequently found in SN-EG than SN-IM and SN-DM, and the prognosis is poor. [3] In addition, extracapsular penetration is one of the poor prognostic factors of HCC, and a

significant difference has been noted in the prognosis between the extracapsular type (5-year survival, 65.6%) and intracapsular type (5-year survival, 80.5%). [20] On EOB-MRI, extracapsular penetration might correspond to a protruding hypointense area from the nodule, which was clearly demonstrated. Ariizumi *et al*. also reported that a non-smooth margin of the tumor, corresponding to SN-EG and CMN in our study, was demonstrated on EOB-MRI and identified as a significant predictor of recurrence with in 1 year after hepatectomy.[13] However, seven of 31 SN-EG nodules were misinterpreted as SN-DM in this study, namely, they were underestimated. This result would be due to thick slice thickness or assessment of the tumor diameter only at the center of the tumor. We believed that this problem could be resolved by assessment of all images with a thin slice thickness because the kappa value of 3-D-GRE group was higher than that of 2-D-GRE group. It should be noted that five of 17 CMN nodules were underestimated, too.

Regarding the tumor size, patients who had tumors that measured 20 mm or less had a significantly better prognosis in comparison with those with larger tumors. [15, 21] Therefore, 20 mm or less was adopted as the cut-off value of tumor-node-metastasis.

Approximately 23 % of the tumors of 20 mm or less were early hepatocellular carcinomas in a large cohort study. [21] In our study, the diameters of SN-IM tumors were significantly smaller and specificity was higher than in the other groups. For this reason, EOB-MRI may predict a good prognosis of SN-IM because a smaller tumor size or SN-IM, so-called early HCC, indicates a good prognosis. [4, 15] There were no significant differences between the three other groups, like in a previous report. [22] In our study, one of 51 nodules 20 mm or less was CMN type HCC, which is associated with a poor prognosis. It is important that a small CMN type HCC be diagnosed correctly by EOB-MRI.

The concordance rate of all nodules showed moderate agreement ($\kappa = 0.45$). The concordance rate was slightly higher when the diameter of the nodules was more than 20 mm ($\kappa = 0.56$), because the diameter of most SN-IM nodules, which were misdiagnosed as SN-DM, were not more than 20 mm.

The limitations of our study include the fact that, first, the MRI systems and scan sequences varied in every institution. This is an unavoidable problem associated with all multicenter studies. Second, the pathological assessment was performed by the

pathologists of each institution. We believed that their pathological assessment was reliable because all pathological diagnoses were based on the same diagnostic criteria provided by the Liver Cancer Study Group of Japan.

In conclusion, Gd-EOB-DTPA-enhanced MRI could predict the macroscopic pathological findings except for SN-IM. Small tumor size might be helpful to diagnose SN-IM. With advances in technology, we will be able to make a more precise diagnosis on thin slice and high-resolution images by carefully reviewing all images.

Acknowledgments

This study was supported in part by Ministry of Health, Labour and Welfare, research on hepatitis and Japanese Health and Labor Sciences research grants for the development of early detection systems of liver cancer using molecular markers and diagnostic imagings.

References

1. El-Serag HB. Epidemiology of hepatocellular carcinoma in USA. *Hepatol Res*.

2007;**37** Suppl 2:S88-94.

2. Japan LCSGo. *General rules for the clinical and pathological study of primary liver cancer, 5th edn*. [book]. 2010:17 - 18.

3. Shimada M, Rikimaru T, Hamatsu T, et al. The role of macroscopic classification in nodular-type hepatocellular carcinoma. *Am J Surg*. 2001;**182**:177-82.

4. Takayama T, Makuuchi M, Hirohashi S, et al. Early hepatocellular carcinoma as an entity with a high rate of surgical cure. *Hepatology*. 1998;**28**:1241-6.

5. Hui AM, Takayama T, Sano K, et al. Predictive value of gross classification of hepatocellular carcinoma on recurrence and survival after hepatectomy. *J Hepatol*. 2000;**33**:975-9.

6. Inayoshi J, Ichida T, Sugitani S, et al. Gross appearance of hepatocellular carcinoma reflects E-cadherin expression and risk of early recurrence after surgical treatment. *J Gastroenterol Hepatol*. 2003;**18**:673-7.

7. Kondo K, Chijiiwa K, Makino I, et al. Risk factors for early death after liver resection in patients with solitary hepatocellular carcinoma. *J Hepatobiliary*

Pancreat Surg. 2005;**12**:399-404.

8. Hatanaka K, Chung H, Kudo M, et al. Usefulness of the post-vascular phase of contrast-enhanced ultrasonography with sonazoid in the evaluation of gross types of hepatocellular carcinoma. *Oncology*. 2010;**78** Suppl 1:53-9.

9. Schuhmann-Giampieri G, Schmitt-Willich H, Press WR, Negishi C, Weinmann HJ, Speck U. Preclinical evaluation of Gd-EOB-DTPA as a contrast agent in MR imaging of the hepatobiliary system. *Radiology*. 1992;**183**:59-64.

10. Huppertz A, Balzer T, Blakeborough A, et al. Improved detection of focal liver lesions at MR imaging: multicenter comparison of gadoxetic acid-enhanced MR images with intraoperative findings. *Radiology*. 2004;**230**:266-75.

11. Bluemke DA, Sahani D, Amendola M, et al. Efficacy and safety of MR imaging with liver-specific contrast agent: U.S. multicenter phase III study. *Radiology*. 2005;**237**:89-98.

12. Hammerstingl R, Huppertz A, Breuer J, et al. Diagnostic efficacy of gadoxetic acid (Primovist)-enhanced MRI and spiral CT for a therapeutic strategy: comparison with intraoperative and histopathologic findings in focal liver

lesions. *Eur Radiol*. 2008;**18**:457-67.

13. Ariizumi S, Kitagawa K, Kotera Y, et al. A non-smooth tumor margin in the hepatobiliary phase of gadoxetic acid disodium (Gd-EOB-DTPA)-enhanced magnetic resonance imaging predicts microscopic portal vein invasion, intrahepatic metastasis, and early recurrence after hepatectomy in patients with hepatocellular carcinoma. *J Hepatobiliary Pancreat Sci*. 2011;**18**:575-85.

14. Nathan H, Schulick RD, Choti MA, Pawlik TM. Predictors of survival after resection of early hepatocellular carcinoma. *Ann Surg*. 2009;**249**:799-805.

15. Ikai I, Arii S, Kojiro M, et al. Reevaluation of prognostic factors for survival after liver resection in patients with hepatocellular carcinoma in a Japanese nationwide survey. *Cancer*. 2004;**101**:796-802.

16. Grazi GL, Cescon M, Ravaioli M, et al. Liver resection for hepatocellular carcinoma in cirrhotics and noncirrhotics. Evaluation of clinicopathologic features and comparison of risk factors for long-term survival and tumour recurrence in a single centre. *Aliment Pharmacol Ther*. 2003;**17** Suppl 2:119-29.

17. Eguchi S, Takatsuki M, Hidaka M, et al. Predictor for histological microvascular

invasion of hepatocellular carcinoma: a lesson from 229 consecutive cases of curative liver resection. *World J Surg*. 2010;**34**:1034-8.

18. Capussotti L, Vigano L, Giuliante F, Ferrero A, Giovannini I, Nuzzo G. Liver dysfunction and sepsis determine operative mortality after liver resection. *Br J Surg*. 2009;**96**:88-94.

19. Pawlik TM, Poon RT, Abdalla EK, et al. Critical appraisal of the clinical and pathologic predictors of survival after resection of large hepatocellular carcinoma. *Arch Surg*. 2005;**140**:450-457; discussion 457-8.

20. Iguchi T, Aishima S, Taketomi A, et al. Extracapsular penetration is a new prognostic factor in human hepatocellular carcinoma. *Am J Surg Pathol*. 2008;**32**:1675-82.

21. Minagawa M, Ikai I, Matsuyama Y, Yamaoka Y, Makuuchi M. Staging of hepatocellular carcinoma: assessment of the Japanese TNM and AJCC/UICC TNM systems in a cohort of 13,772 patients in Japan. *Ann Surg*. 2007;**245**:909-22.

22. Choi GH, Han DH, Kim DH, et al. Outcome after curative resection for a huge

(>or=10 cm) hepatocellular carcinoma and prognostic significance of gross tumor classification. *Am J Surg*. 2009;**198**:693-701.

Table and Figure legends

Table 1 Correlation between pathologic and MR findings

		Macroscopic types by MR findings					
		n	SN-IM	SN-DM	SN-EG	CMN	IF
Macroscopic types by pathological findings	SN-IM	19	1	15	1	2	0
	SN-DM	79	1	67	7	3	1
	SN-EG	31	0	7	18	6	0
	CMN	17	0	3	2	12	0
	IF	0	0	0	0	0	0
	Total	146	2	92	28	23	1

CMN, confluent multinodular type; IF, infiltrative type; MRI, magnetic resonance imaging; SN-DM, simple nodular type (with distinct margin); SN-EG, simple nodular type with extranodular growth; SN-IM, small nodular type with indistinct margin.

Table 2 Statistics of each macroscopic type

	SN-IM			SN-DM			SN-EG			CMN		
	≦20 (n=16)	>20 (n=3)	total (n=19)	≦20 (n=27)	>20 (n=52)	total (n=79)	≦20 (n=7)	<20 (n=24)	total (n=31)	≦20 (n=1)	<20 (n=16)	total (n=17)
Sens	6.3	0	5.3	85.1	84.6	84.8	57.1	58.3	58.1	100	68.8	70.6
Spec	50	100	99.2	33.3	79.1	62.7	93.2	90.1	91.3	96.0	88.6	91.5
Accu	68.6	96.8	87.0	60.8	82.1	81.4	88.2	82.1	84.2	96.1	85.3	89.0
NPV	69.4	96.8	87.5	66.7	81.0	80.8	93.2	86.5	88.9	100	93.3	95.9
PPV	50.0	0	50.0	59.0	83.0	72.8	57.1	66.7	64.3	33.3	55.0	52.0

Accu, accuracy; CMN, confluent multinodular type; NPV, negative predictive value; PPV, positive predictive value; Sens, sensitivity; SN-DM, simple nodular type with distinct margin; SN-EG, simple nodular type with extra-nodular growth; SN-IM, small nodular type with indistinct margin; Spec, specificity.

Fig. 1 Summaries of the five macroscopic types of hepatocellular carcinoma.

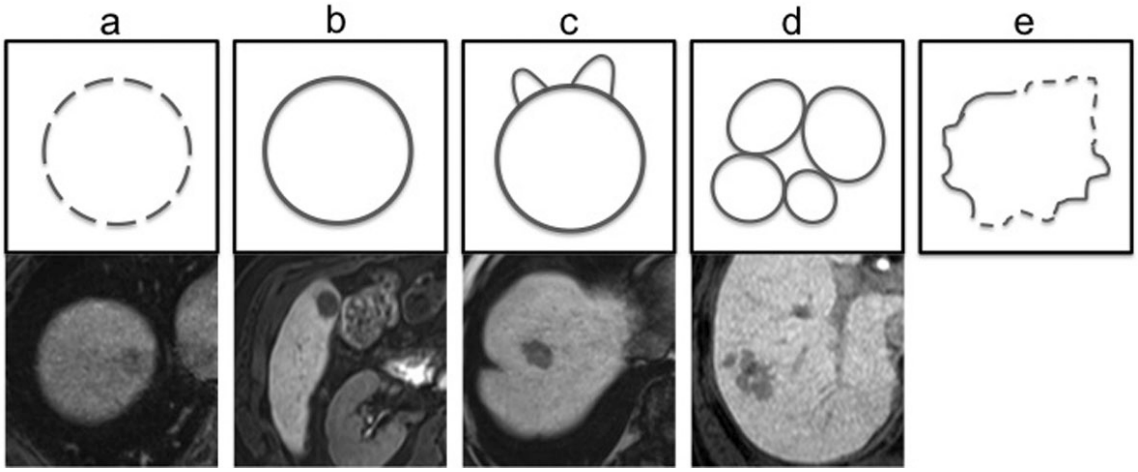

Top Schemas. *Bottom* hepatobiliary phase images of gadolinium-ethoxybenzyl-diethylenetriamine pentaacetic acid-enhanced MRI. (a) Small nodular type with indistinct margin. (b) Simple nodular type with distinct margin. (c) Simple nodular type with extranodular growth. (d) Confluent multinodular type. (e) Infiltrative type (there was no case of this type in this study).

Fig. 2 Correlation of the diameter between macroscopic findings and magnetic resonance (MR) findings

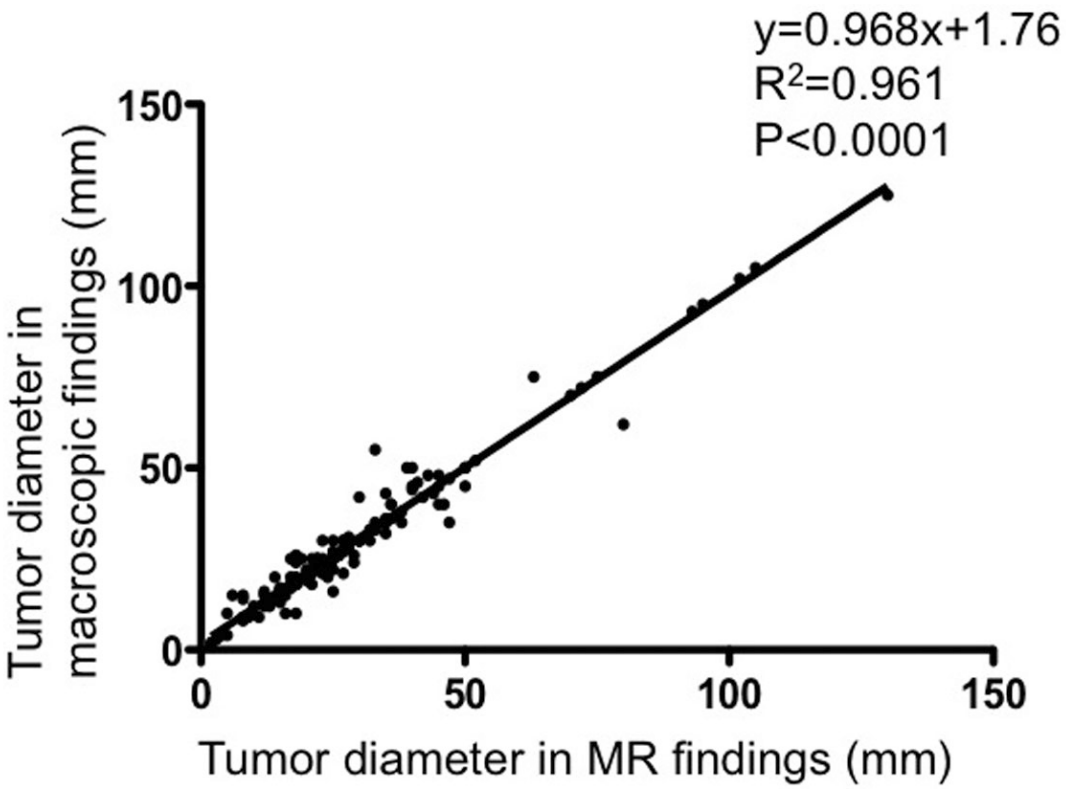

Fig. 3 The tumor diameter of each group on MR images

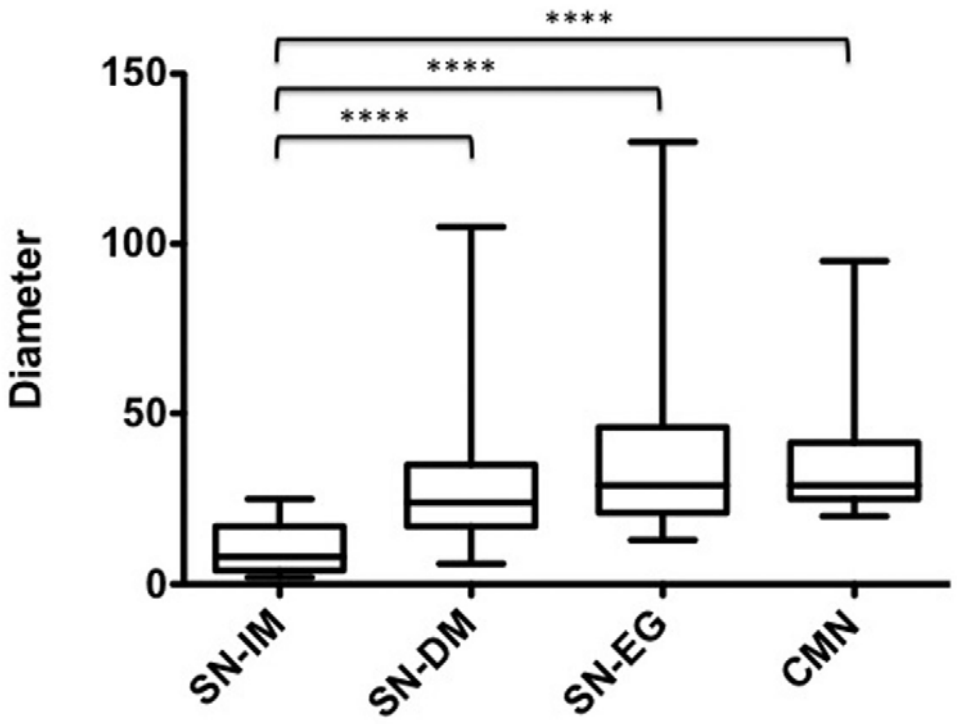

Boundary of box closest to zero, 25th percentile; line in boxes, median; boundary of boxes farthest from zero, 75th percentile; error bars, minimum and maximum value; ****, $P < 0.0001$. SN-IM, small nodular type with indistinct margin; SN-DM, single nodular type with distinct margin; SN-EG, single nodular with extra-nodular growth type; CMN, confluent multinodular type